ORIGINAL RESEARCH ARTICLE

Gallium-Based Liquid Metal Flexible Electronics Prepared by Solid–Liquid Phase Transition

Yan Zhu[1] · Xilong Ding[1] · Yunpeng Jiang[1]

Abstract

A facile fabrication method of pure gallium-based flexible electronics has been developed by using the solid–liquid phase transition at ambient temperature, effectively broadening the application of traditional processing techniques in these stretchable devices. The key point of this work is to make ductile Ga-based liquid metal wires, which exhibit superior mechanical properties with a tensile strength of 30 MPa and a break strain higher than 10%. Their fracture mechanisms were successfully investigated with their fracture morphology and Schmid's law. Some electronic devices were prepared by patterning Ga-based wires in the form of U-shape, S-shape, and spiral shapes, and tested to obtain the variation in their structural resistance with stretching. Finite element method (FEM) simulations with the COMSOL code and analytical predictions were also performed to elucidate their piezo-resistance effect, and a good agreement among these predictions were reached. The present fabrication technique is of high simplicity, high efficiency, high quality, mass production, and low cost in making high-resolution, highly conductive, and three-dimensional flexible electronic devices.

Keywords Gallium-based liquid metals · finite element method (FEM) · processing · solid–liquid phase transition · flexible electronics

Introduction

Gallium-based liquid metals (Ga-based LMs) have a high boiling point (> 2000°C), high electronic conductivity (~ $10^6/\Omega$ m), high thermal conductivity (× 60 times water), self-healing, and nontoxicity, and are endowed with many potential applications in new energy, advanced manufacture, thermal management, civil engineering, flexible intelligence, and biomedical engineering.[1–4] Therefore, it is very important to develop a sophisticated method for preparing Ga-based electronics to meet the exacting demands of these industries.

Ga-based LM patterning in a soft matrix[5] is an important prerequisite in preparing soft composites[6] and their flexible electronics.[7] At the present time, the prevalent processing techniques are stirring-mold casting,[8] microfluid control,[9] and three-dimensional (3D) printing.[10–14] Recently, some appealing fabrication methods, such as micro-transfer molding[15] and solidified LM manufacture,[16] have gradually been put forward. For instance, using an external electronic field, temperature, and mechanical force to push the LM solution forward over the whole pattern domain in the microfluid control processing, and precise control and operation of LM droplets along these micro-tunnels, have been realized.[17–20] The main defects of microfluid control processing are: firstly, some complicated procedures, such as soft lithography and spray and laser carving techniques, are utilized to make microstructures on the surfaces of soft substrates, which causes the manufacture cost to be relatively high. Additionally, the alignment errors in gathering the upper and down molds are very hard to control. Secondly, microtunnels size are very minute, which results in high resistance in LM flowing through the microchannels, which are very easily blocked by some residue micropowders or air bubbles in the LM solutions. Thirdly, the input and outlet sites should be predesigned and preformed on the surfaces of the molds to connect the LM sink and vacuum pump, respectively. After the fabrication of flexible electronics, these sites should be carefully sealed with adhesive tape, but the regions are still weak points for LM leakage during the application. And fourthly, the mold texture should be rigid

✉ Yunpeng Jiang
  ypjiang@nuaa.edu.cn

1 College of Aerospace Engineering, Nanjing University
  of Aeronautics and Astronautics, Nanjing 210016, China

to avoid the structural collapse of the whole microchannel cavum during the vacuum suction process.

In the stirring-mold casting process, LMs and elastomer solution are mechanically mixed at a predesigned volume ratio to obtain a homogeneous emulsion, and then poured into a specified mold for curing at room temperature or in a vacuum oven.[21,22] This method is very simple, highly efficient, and suitable for most ingredients. However, Ga-based LMs are approximately 6.44 g/cm^3, nearly 6 times that of polydimethylsiloxane (PDMS) or Ecoflex elastomers. Consequently, the LM droplets easily sink in the mixed emulsion, leading to it being elastomer-rich at the top and LM-rich at the bottom, which corresponds to it being insulating in the upper part and conductive in the down part. It is still a challenging issue to prepare uniform LM composites by this method. The common defects in the mold-casting technique can be summarized as, firstly, the LM droplets sink rapidly in elastomer solutions due to their high density, low viscosity of silicone solvents, and a relatively long curing period. Therefore, the prepared composites are not uniform in their microstructures, and thus the isotropic performance in their mechanical and electronic behaviors is hard to achieve. And, secondly, an inevitable procedure of mechanical sintering is required for the as-received LM composites in order to realize their conductive function from the initial insulated state. Unfortunately, LM droplets are apt to leak and contaminate the surrounding components under the applied pressure, even leading to short circuits in some electronics due to their high fluidity and finite deformation of soft substrates. Therefore, an extra leakage-proof structure should be appended in most cases.

The 3D printing technique uses shear thinning and deposition forming to directly shape some complicated LM patterns on a variety of substrates, and high-resolution precast molds are not needed.[23] Liu et al. developed a one-step dual-material 3D printing method for an elastomer lattice, where a 3D interconnected LM network was held by a highly regular PDMS lattice skeleton. The composite exhibited excellent electromagnetic interference shielding effectiveness (72 dB).[24] However, 3D printing has the following weaknesses. Firstly, LM droplets tend to be spherical during the printing process due to their low viscosity and high surface tension, and their easily reacted Ga$_2$O$_3$ film at ambient environment significantly restricts their fluidity, which induces many more droplets near the printer nozzle than near the formed filament, and it becomes very hard to form a continuously tunable integrated circuit. Secondly, the adhesive strength between the printed LM paste and smooth substrates is too low to induce debonding and functionality loss. Thirdly. the quality of the LM patterns strongly relies on the printing parameters, such as nozzle diameter, distance between the nozzle and substrates, applied pressure, and traveling speed of the nozzle. And, fourthly. hitherto, the

3D printing technique has been limited to making 2D electronic circuits, and making 3D integrated electronics has not yet been realized. What is more, the total cost of maintaining the printing equipment is very high in mass production.

In the light of the above literature survey and the existing deficiencies in these techniques, the objective of this work is to develop a highly efficient method to fabricate flexible electronics by using a solid–liquid phase transition at ambient temperature for Ga-based alloys. In the Section "Experiments", we present the preparation methods of Ga-based LM wires, typical wire patterns, and their electronic devices. Finite element method (FEM) simulations and analytical models are then conducted in Section "Theoretical Models". The results of both the measured and simulated fracture mechanisms under tension are given in Section "Results and Discussion". The merits, weaknesses, and potential applications of the developed technique is discussed in Section "Merits and Demerits of this Technology". The conclusions are finally summarized in Section "Conclusions".

Experiments

Materials

High-purity gallium supplied by Changsha Kunyong New Materials (Sylgard-184; Dow Corning) was used for the package coating of the LM wires and their patterns, and mixed with the curing agent, as described in the technical note, and thermally cured at 100°C for 1 h. Ethanol with a chemical purity of 99.7% was supplied by Chinasun Specialty Products, and PTFE (polytetrafluoroethylene) capillaries with three different inner diameters were purchased from Shanghai Beft Rubber Products. Copper conducting wires were used as guide wires in testing the flexible electronics. Three specimens of each composition were tested and the average value reported, and the measured stress–strain relationships of PDMS under tension and compression are shown in Figs. S1 and S2 (see online supplemental material), respectively.

Fabrication of LM wires

Figure 1 shows the fabrication procedures of the LM wires and the resulting flexible electronics. Since the melting point of pure gallium is 29.8°C, the water bath method was used to dissolve the solid gallium. PTFE capillaries were selected to inject liquid LM due to their low friction coefficient of 0.06, high tensile strength of 20–35 MPa, and high stretchability of 200–400%. Liquid gallium was easily vacuum-infused into a PTFE capillary 2 m in length and 0.3 mm in inner diameter by a syringe, and then the two ends of the capillary were sealed with adhesive tape. A refrigerator at
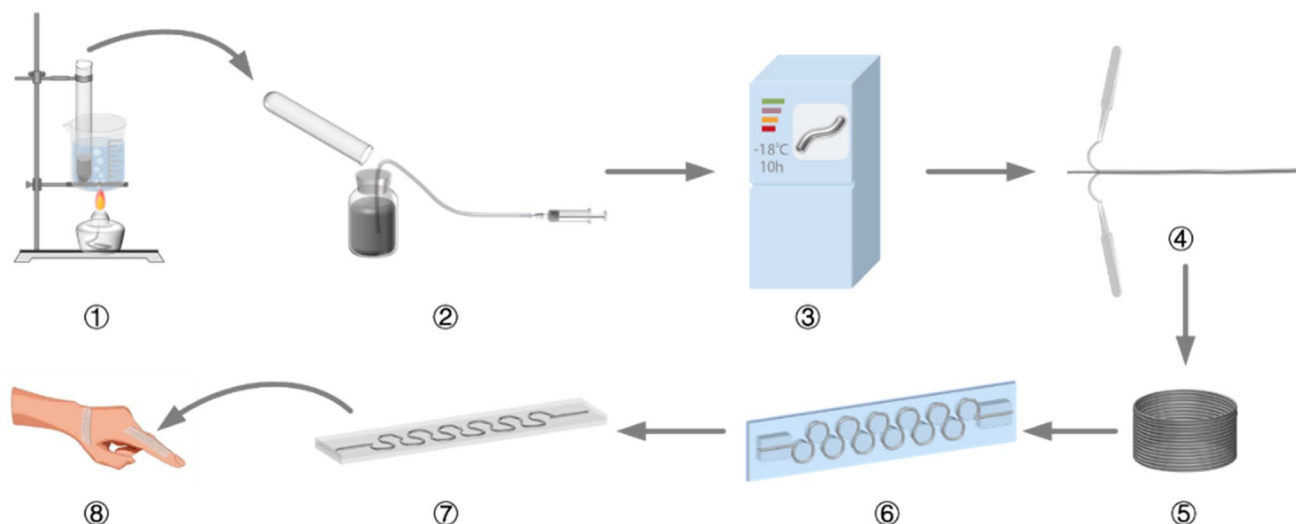
Fig. 1 Fabrication methodology of LM wire and flexible electronics: (1) melting of LM, (2) infusion, (3) freezing, (4) peeling off, (5) LM wire ring, (6) LM patterning, (7) fabrication of flexible electronics, and (8) application.

a temperature of − 18°C was used to freeze the liquid LM in the PTFE capillary for 10 h. Finally, one end part of the capillary was split with scissors, and then the two parts of the capillary were separately clamped by tweezers to peel the remaining part. Finally, an intact LM wire was successfully achieved, as shown in Fig. S3.

Preparation of Electronic Devices

Ultraviolet curable resin was adopted to make high-resolution molds with U-shape, S-shape and coaxial spiral patterns by using the 3D printing technology, and a conical degree of 5° was introduced in these patterning molds for easy demolding (see Fig. S4). The lubricating agent was firstly sprayed on the printed mold surfaces, and, after 10 min, the LM wires were shaped into the specified patterns on the mold (see Fig. S5), and then the patterned wires were transferred to be encapsulated with PDMS solution.

PDMS was used as a soft matrix of the flexible electronics, part A and curing agent were mixed at the weight ratio of 1:10 for 5 min, and air bubbles were degassed by vacuuming for 10 min, finally being poured into a preformed silicone mold for curing in an oven at 100°C for 30 min. The prepared PDMS film of 0.35 in thickness was used as a bottom film, on which the patterned LM wires were placed flat, and then the PDMS solution was cast to cover the LM wires. After the curing, the as-prepared flexible electronics was used for the next tests (see Fig. S6).

Tension Test

Figure 2 shows the experimental set-up for measuring the mechanical and electronic behaviors of the LM electronics.
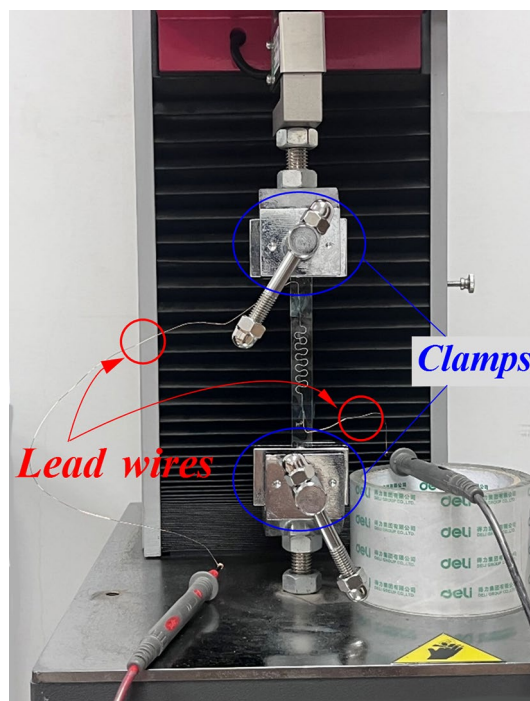

Fig. 2 Schematic of the set-up for mechanical–electronic testing.

Uniaxial tension tests were performed according to ASTM D638 to measure the tensile properties of the LM wires, PDMS, and flexible electronics using a hydraulic-driven testing machine (3365 series; Instron; Boston, USA) and data acquisition card AD12 (Contec, Japan). Uniaxial tension tests are carried out using a hydraulic-driven Instron tension tester at a constant crosshead displacement speed of 1 mm/min at room temperature, according to ASTM D3039

used for testing tensile properties of polymers. The displacement with a gauge length of 50 mm was attached to the specimen to measure the average longitudinal strain for the PDMS samples.

Theoretical Models

Analytical Model of Resistance Variation

The analytical models were used to predict the variation of resistance with the applied stretch ratio for the LM wire patterns shown in Fig. 3. According to Pouillet's law, together with the incompressibility of LM and elastomer matrix,[25] the normalized resistances with stretch ratio, ε, are expressed as follows after the necessary mathematics deductions,

For the U-shape pattern:

$$R/R_0 = \begin{bmatrix} 20(1+\varepsilon) + \dfrac{45.6}{\sqrt{1+\varepsilon}} + \\ 24 \times \displaystyle\int_0^{\frac{\pi}{2}} (1+\varepsilon)r\sqrt{1+(1+\varepsilon)^3\tan^2\theta} \cdot \cos\theta \, d\theta \end{bmatrix} \times (1+\varepsilon) \quad (1)$$

For the S-shape pattern:

$$R/R_0 = \left[48 \times \int_0^{\frac{\pi}{2}} (1+\varepsilon)r\sqrt{1+(1+\varepsilon)^3\tan^2\theta} \cdot \cos\theta \, d\theta \right] \times (1+\varepsilon) \quad (2)$$

For the spiral-type pattern:

$$R/R_0 = \left[10(1+\varepsilon) + \int_0^{6\pi} 2(1+\varepsilon)\sqrt{1+\left[\frac{dy}{(1+\varepsilon)^3 dx}\right]^2} \, dx \right] \times (1+\varepsilon) \quad (3)$$

where ε denotes the applied strain along the loading direction. The detailed deductions about Eqs. 1–3 can be found in the supporting materials.

Numerical Simulations

The elastomer matrix and Ga-based LMs are supposed to be isotropic, nonlinear, hyperelastic solids, both being characterized by the Neo-Hookean hyper-elastic constitutive equation consisting of deviatoric strain energy regardless of volume deformation and hydro-strain energy related to the volume ratio, J, and expressed by:

$$W = \frac{\mu}{2}(\bar{I} - 3) + \frac{\kappa}{2}(J-1)^2 \quad (4)$$

where $\bar{I}$ is the deviatoric strain invariant that is defined as $\bar{I} = J^{-2/3}I_1$, strain invariant $I_1 = \lambda_1^2 + \lambda_2^2 + \lambda_3^2$, and λ_1, λ_2 and λ_3 are the stretch ratios in the principal stress directions of 1, 2, and 3, respectively, and J denotes the volume ratio of the body before and after deformation and defined as $J = \lambda_1\lambda_2\lambda_3$. The value $J = 1$ for the incompressible materials. The elastomer and Ga-based LMs are usually incompressible, but these assumptions are approximations of reality. Moreover, a minute change in the volume would have a significant effect on their responses. Additionally, their compressibility adopted in the FEM analysis could achieve an easier convergence in the iterative process. Therefore, $J \neq 1$ is employed in the present model for the elastomer and LMs, and μ and κ are the shear and bulk moduli, expressed in terms of the elastic modulus, E, and Poisson's ratio, ν, as $\mu = E/2(1 + \nu)$ and $\kappa = E/3(1 - 2\nu)$. Since Ga-based LMs are fluid, the shear modulus $\mu_{LM} \to 0$ and the bulk modulus $\kappa_{LM} \approx 10^9 \sim 10^{10}$ GPa, while the shear and bulk moduli of the elastomers are $\mu_{elast} \approx 0.1$–10 MPa and $\kappa_{elast} \approx 10^9$ GPa, respectively.[26] The wide difference between them is so high that the convergence in the iterative process is not reached. The COMSOL commercial software[27] was employed to analyze the mechanical and electrical behaviors under the
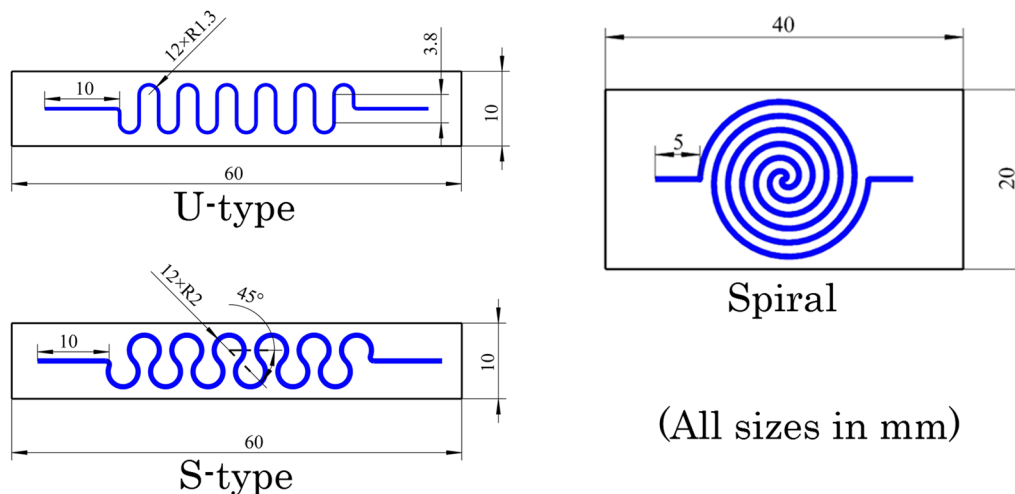

Fig. 3 Geometry and sizes of U-shape, S-shape, and spiral electronics (dimensions in mm).

stretching for these prepared electronics, and the material properties used are listed in Table I.

3D FEM models were adopted in the COMSOL software to analyze the electronic behaviors of the flexible devices with the applied deformation. In the AD/DC module, boundary conditions were imposed as follows: the left side of the FEM model was fixed along the tensile direction, and linked to the ground, while the right side was stretched to a certain strain, and assigned the current value of 10 A, whereby the voltage potential was obtained to compute the structure resistance, R. A physics-controlled mesh was used to make the model discrete, and solid elements were used for the mesh, and their number was increased until the convergence was reached.

Results and Discussion

Mechanical Properties of Ga-Based LM Wires

The fabricated LM wires could be readily molded into the periodic patterns of U-shape, S-shape, and spiral shape, as shown in Fig. 4a, b, and c, respectively, and the interspaces between the wires were 2.3 mm, 1.36 mm, and 1.32 mm, respectively. Additionally, the abbreviation of Nanjing University of Aeronautics and Astronautics (NUAA) was also shaped in Fig. 4d. All these patterns demonstrated that the prepared LM wires have high malleability, good strength, and superior surface quality at the same time.

The influence of wire diameter on the mechanical properties was demonstrated by the typical stress versus strain curves shown in Fig. 5a. A large plastic deformation appears for these LM wires under uniaxial tension. The necking effect is very evident at the yielding stage, which is associated with a big yield tooth in these stress–strain curves. As the stress exceeds the yielding stress, the deformation responses step into a long-range plateau stage accompanied by the propagation of many more serried slipping bands along the stretching direction.

The tensile strength and strain at failure of the cylinder LM wires strongly rely on their initial diameters, as shown in Fig. 5b. The results indicated that both the break strength and elongation increase with increasing wire diameter. What is most impressive is that the fracture morphology in these samples is very peculiar, in stark contrast to those of traditional metals. Based on the surface observation of these fractured specimens shown in Fig. 6, all the samples have

a necking effect, marked plasticity accompanied by evident slip bands, and final breaking at an angle of 38° against the tensile direction. The biggest difference between these samples lies in the number density of the slip bands. For the 0.3-mm wires, the slip bands are dilute and their fracture surface is relatively flat; for the 0.6-mm wires, many more slip bands nucleated, and their fracture surface is very curvy, implying much more energy dissipated during the elongation; and for the 1-mm wires, many more dense parallel slip bands appear in the necking region. These outward features are also in good accordance with their plasticity displayed in the stress versus strain relationships.

Based on the observation of the fractured samples, their corresponding toughening mechanism can be explained by Fig. 7.
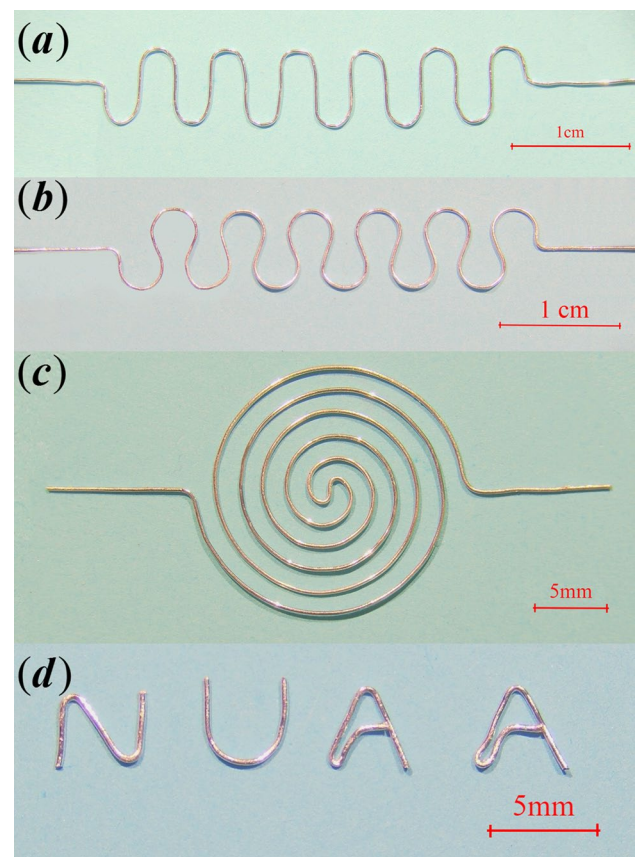

Fig. 4 The prepared patterns of Ga-LM wires in the shapes of U (a), S (b), spiral (c), and NUAA logo (d), and images showing the stretchability of the as-prepared stretchable conductors.

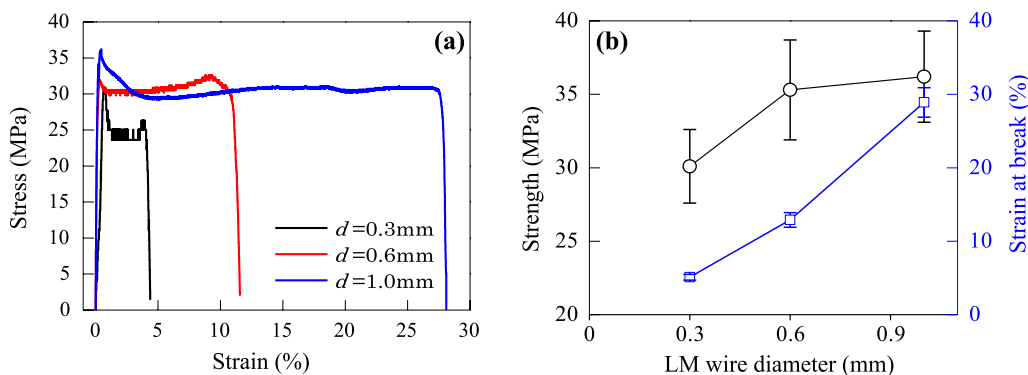| Table I Material properties of constituents		E (MPa)	ν	ρ (kg/m^3)	μ (kPa)	κ (MPa)	σ (S/m)
	LM	0.1	0.49	6440	1 [26]	50 [26]	10^4 [26]
	PDMS	1.5 [28]	0.49	970	100 [26]	10 [26]	1 [26]

Fig. 5 Stress–strain relationships of three sizes of LM wires (a) and dependence of tensile strength and elongation on wire diameters (b).
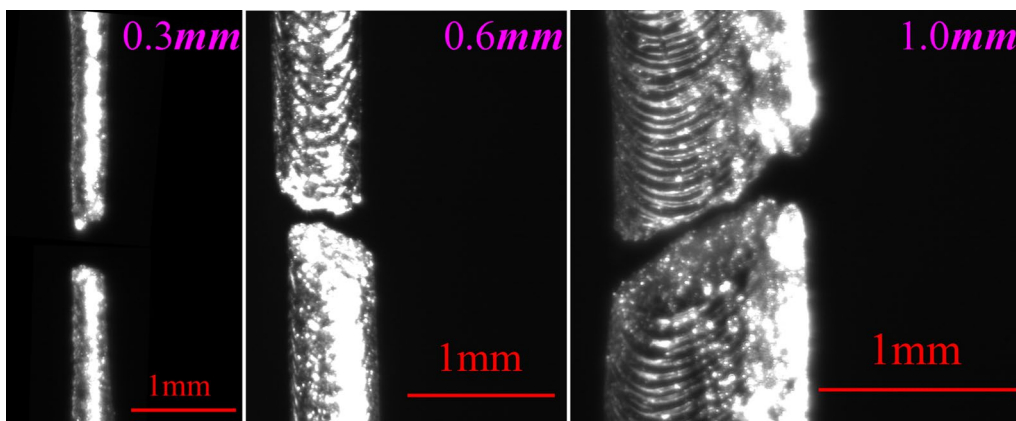

Fig. 6 Slip bands on three different LM wires.

At the very beginning stage, the Ga-LM wire is subjected to linear elastic state until the yielding point, where there is a shear band across the cross-section of the wire sample shaped at an angle of 45° with respect to the tensile direction. A further stretch would lead to the rotation of slipping bands toward the stretching direction, which is confirmed by observing that the minimum cross-section appearing in the oval shape from the vertical view, while the elliptical shape is gradually elongated with further stretching. The specific fracture mechanism is explained in Fig. 7. According to Schmid's law,[29] the shear stress on the slip plane along the slip direction is:

$$\tau = \sigma \cos \alpha \cos \beta \qquad (5)$$

where σ is the axial normal stress, α is the angle between the tensile and slip directions, β the angle between the tension normal to the slip plane. As $\beta = 45°$, the maximum shear stress, $\tau_{max} = \sigma/2$, is reached, and the orientation is the most favorable direction for slipping. As τ reaches a threshold, τ_C, the crystal boundary will slip whatever the texture orientation of the samples against the loading direction.
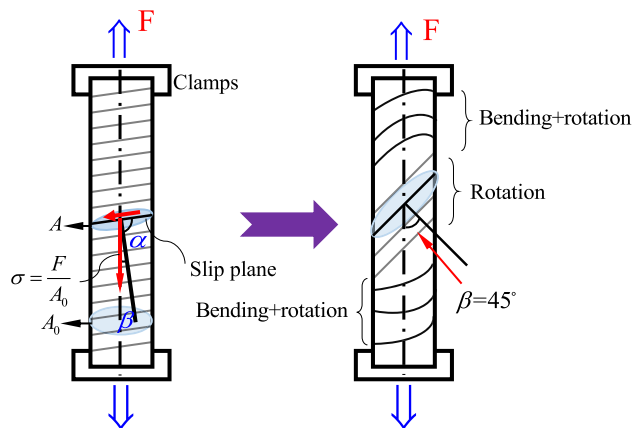

Fig. 7 Toughening mechanism of LM wires.

After the slip bands start, the testing sample should rotate toward the loading direction due to the boundary constraint from the clamps of the testing machine, and thus the primary slip planes rotate toward the loading direction. The

variation of slipping direction changes the primary crystal plane from favorable to unfavorable slipping after a period of slipping, while the primary crystal planes unfavorable for slipping will rotate to the direction of favorable for slipping, and subsequently take part in slipping. Consequently, the alternatively propagated slip systems in different directions bring about the uniform stretching of the specimens. With a further extension, the diameter of a portion of the LM wire begins to decrease abruptly due to the local instability in deformation. Finally, we note that rupture occurs along the oblique section that forms an angle of approximately 45° with the original surface of the specimens. This implies that shear stress along the diagonal plane is primarily responsible for the fracture of the ductile materials. The wire diameter greatly affects the distribution and density of the slip bands, and the much thicker slip bands experienced during the deformation correspond to a higher plastic elongation and higher fracture toughness.
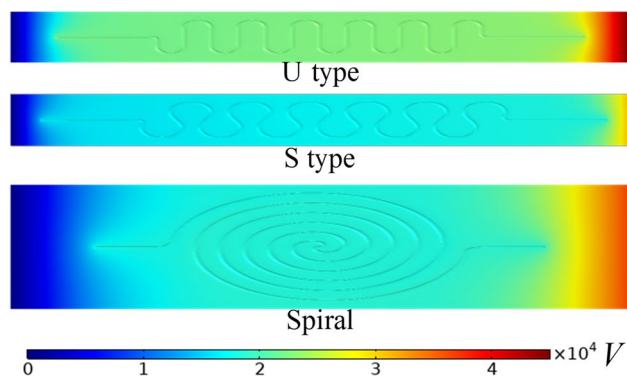
Analytical Results and Simulations

Figure 8 shows the simulation results of the electrical potential distribution of electronic devices under an elongation of 100%. This figure demonstrates the electric potential distribution in the devices with varied patterns, from which their resistance can be compared with each other. As the color changes from blue to red, the electrical potential increases exponentially. The higher the color gradient, the higher the pattern resistance of the LM interconnect. It is noted that the gradient of the U-shape is the highest, and that of the S-shape is the lowest among these cases. The color contours in the central parts of these devices are uniform, resembling the periodical structures of these interconnects. The resistances of the interconnects under different strains have been calculated according to the drop of electrical potential.

The predicted resistance variation with strain by the FEM simulations and analytical models are plotted in Fig. 9a, and compared with the measured results for these varied patterns. Both he U-shape and S-shape patterns exhibit a negative piezo-resistance effect for a strain less than 40%, and then change to be positive, while the spiral-type presents a positive effect in the whole elongation. Jiang[30] studied the orientation effect of LM chains on the resistance variation, and found that the LM chain structure exhibits a negative piezo-resistive effect as the LM chain becomes perpendicular to the stretching direction, which was accurately predicted by the developed theoretical model. At the beginning stage of stretching the U-shape and S-shape patterns, the rotation of the winding LM wires consists of the structural deformation, and most of the vertical parts of the LM wires contribute to the negative piezo-resistive effect, as depicted in Fig. 9b. It is noted that the U-shape and S-shape patterns show relatively similar structures, which can be described by the same analytical model with a subtle difference in geometric sizes. A reasonable agreement was reached between the FEM modeling and the theoretical predictions at the strain
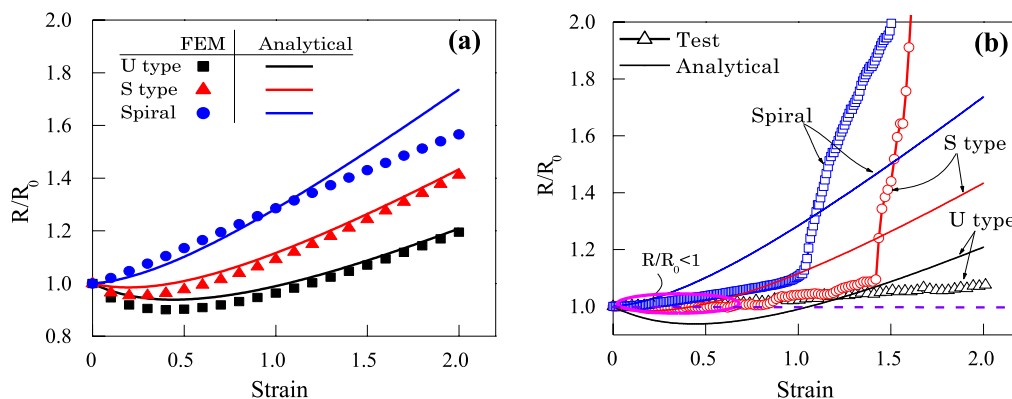

Fig. 8 Simulation results of the electrical potential distribution of the U-shape, S-shape and spiral-type devices at the stretch ratio of 100%.

Fig. 9 The normalized resistance variation with strain: by FEM simulation and analytical models (a) and the measured results (b).

up to 200%. The prediction error in the spiral type becomes larger and larger after exceeding 120% of strain, which originates from the incompatible deformation between adjacent wire paths due to their complicated pattern.

Based on the measured resistance variation with applied strain in Fig. 9b, the resistance first decreases in the very beginning stage of deformation for the U-shape and S-shape patterns (the marked circle indicates $R/R_0 < 1$), which is in accordance with those predicted by the FEM simulations and analytical predictions. The predictions by the analytical model are also plotted with the testing results, and the comparison demonstrates that a large deviation was found for the spiral case. The main reason lies in their complicated shape variation in the stretching process, which could not be well considered in the developed theoretical model. The variation rate of resistance with extension of these wire patterns are: U-shape < S-shape < spiral, which reaches a good agreement among the experiments, theoretical predictions and FEM modeling. In addition, the maximum variation rate, R/R_0 is less than 2.0 in the predictions and testing results, indicating that the developed analytical models and FEM simulations are accurate in capturing the main characteristics of the LM electronics. Their great potential for applications are demonstrated by some associated videos for these flexible electronics in the supporting materials. The drastic increases in the resistance of the S-shape and spiral patterns seem very unreasonable, while the resistance variation in the U-shape case is more normal. The possible reasons lie in the loose connection between the Cu lead wires and LM electronics during the applied stretching, while the local damage in the

LM conductive path also impairs the electric conductivity of the whole devices.

Merits and Demerits of this Technology

To demonstrate the superior conductivity of these electronics, the LM wire patterns were encapsulated in silicone rubber, and mechanical sintering was not required to activate the conductivity. The obtained circuit could maintain its functionality and integrity under different loading modes, such as stretching, bending, and twisting for these interconnects, as shown in Fig. 10. The light-emitting diodes (LEDs) displayed a constant brightness when the electronic circuits were subjected to arbitrary deformations. Compared with other preparation methods for Ga-based LM electronics, the present processing method has the following advantages:

(1) Based on the low melting point feature of Ga-based LMs, the phase transition between the solid and liquid states could be realized with great convenience at room temperature. The solid LM wires could be readily constructed for some complicated electronic devices, and then their functionalities used in their liquid state to satisfy their predetermined objectives. In conventional material processing, high-temperature melting or complicated forging are usually demanded, which is in stark contrast to the present technique. Therefore, the present production cost is very low, and the preparation is easily mass produced, presenting a high efficiency relative to more traditional techniques.
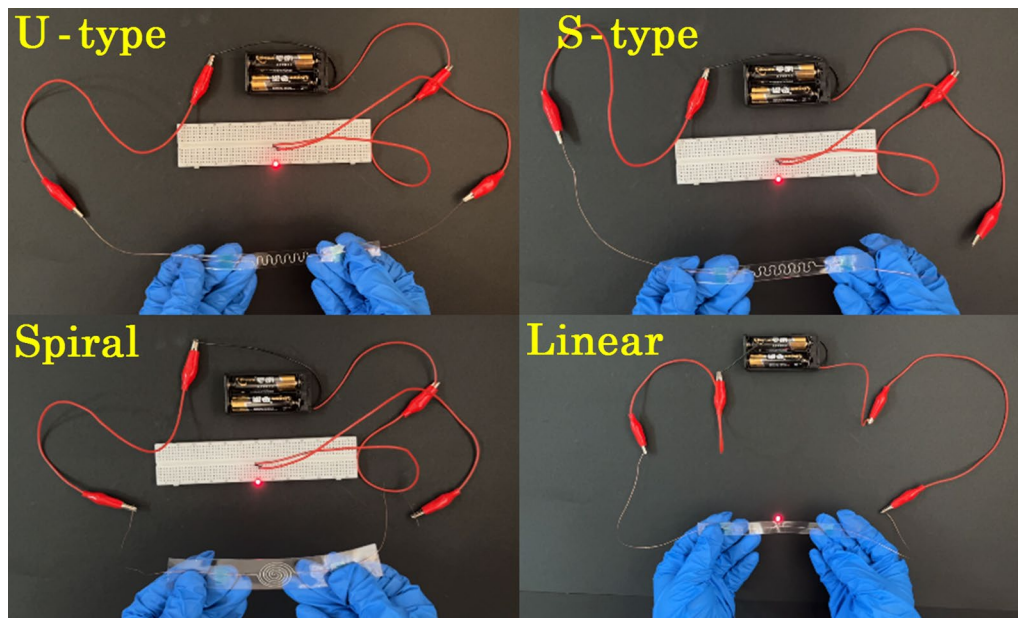

Fig. 10 Stretchable circuits to conduct a LED with various patterns.

(2) The whole processing is very simple, highly efficient, and mass produced. Advanced equipment of high grade and precision are not required, and therefore this technique is very applicable for small-scale companies or individuals.

(3) The LM sedimentation and leakage[31,32] usually occurring in the conventional mixing–casting process was avoided, and thus the corresponding negative impact on the material properties was excluded, so that the as-prepared electronic devices have high functional stability.

(4) This technique can break the restrictions of conventional methods using 2D plane electronics, helping us to make complicated, highly compacted 3D electronic structures.[16] Not only are the spatial dimensions in designing the scope of electronic circuits enriched but an alternative possibility to make highly advanced and more powerful electronic devices has been demonstrated

(5) Ga-based LM flexible electronics prepared by this method are highly conductive, of high resolution and superior malleability, and also have a low production cost, so paving the way for commercializing these LM-based electronics in the near future.

On the other hand, it is noteworthy that some deficiencies in the present technique should be further improved. The peeling process readily impairs the smooth surface of the LM wires, and need to be auto-machined in the future. The most serious issue in preparing LM electronics is how to firmly connect the outer lead wires in their application. The minimum sizes of the electronic devices we could fabricate are only 0.3 mm at the present time, and thus much more delicate components should be engineered with the present technique.

Conclusions

We have provided a facile and efficient technology to fabricate Ga-based LM stretchable electronics using their solid–liquid phase transition at ambient temperature. Additionally, the mechanical and electronic responses of these fabricated flexible electronics were measured under large deformations, and the testing results were correlated with FEM simulations and analytical predictions, whereby the piezo-resistive mechanisms in these devices with three typical LM patterns have been clearly elucidated. The present technique is very simple, highly efficient, mass-produced, and inexpensive in preparing high-resolution, highly conductive, and 3D flexible electronics. The solid–liquid phase transition of Ga-based LMs may play an important role in the future design of stretchable electronics, soft robots, and multi-functional devices.

Data availability The data that support the findings of this study are available from YPJ upon reasonable request.

Conflict of interest No potential conflict of interest was reported by the authors.

References

1. M.D. Dickey, A river (of liquid metal) runs through it. *Natl. Sci. Rev.* 7, 721 (2020).
2. M.K. Zhang, S.Y. Yao, W. Rao, and J. Liu, Transformable soft liquid metal micro/nanomaterials. *Mater. Sci. Eng. R* 138, 1 (2019).
3. K. Kalantar-Zadeh, J.B. Tang, T. Daeneke, A.P. O'Mullane, L.A. Stewart, J. Liu, C. Majidi, R.S. Ruoff, P.S. Weiss, and M.D. Dickey, Emergence of liquid metals in nanotechnology. *ACS Nano* 13, 7388 (2019).
4. M.K. Zhang, S.Y. Yao, W. Rao, and J. Liu, Transformable soft liquid metal micro/nanomaterials. *Mat Sci Eng R* 138, 1 (2019).
5. M.W. Kim, H.J. Lim, and S.H. Ko, Liquid metal patterning and unique properties for next-generation soft electronics. *Adv. Sci.* 10, 2205795 (2023).
6. S. Chen, H.Z. Wang, R.Q. Zhao, W. Rao, and J. Liu, Liquid metal composites. *Matter* 2, 1446 (2020).
7. I.D. Joshipura, H.R. Ayers, C. Majidi, and M.D. Dickey, Methods to pattern liquid metals. *J. Mater. Chem. C* 3, 3834 (2015).
8. N. Zolfaghari, P. Khandagale, M.J. Ford, K. Dayal, and C. Majidi, Network topologies dictate electromechanical coupling in liquid metal-elastomer composites. *Soft Matter* 16, 8818 (2020).
9. L.N. Song, W.R. Gao, and Y. Rahmat-Samii, 3-D printed microfluidics channelizing liquid metal for multipolarization reconfigurable extended *E*-shaped patch antenna. *IEEE T. Antenn. Propag.* 68, 6867 (2020).
10. J.X. Ma, Z.H. Liu, Q.K. Nguyen and P. Zhang. Lightweight soft conductive composites embedded with liquid metal fiber networks. *Adv. Funct. Mater.* 2308128 (2023)
11. Y. Zheng, Z.Z. He, Y.X. Gao, and J. Liu, Direct desktop printed-circuits-on-paper flexible electronics. *Sci. Rep.* 3, 1786 (2013).
12. Y. Zheng, Z.Z. He, J. Yang, and J. Liu, Personal electronics printing via tapping mode composite liquid metal ink delivery and adhesion mechanism. *Sci. Rep.* 4, 4588 (2014).
13. C. Ladd, J.H. So, J. Muth, and M.D. Dickey, 3D printing of free standing liquid metal microstructures. *Adv. Mater.* 25, 5081 (2013).
14. Y.X. Gao, H.Y. Li, and J. Liu, Direct writing of flexible electronics through room temperature liquid metal ink. *PLoS ONE* 7, 45485 (2012).
15. M.G. Kim, H. Alrowais, and O. Brand, 3D-integrated and multifunctional all soft physical microsystems based on liquid metal for electronic skin applications. *Adv. Electron. Mater.* 4, 1700434 (2018).
16. G.Q. Li, M.Y. Zhang, S.H. Liu, M. Yuan, J.J. Wu, M. Yu, Z.W. Xu, J.H. Guo, G.L. Li, Z.Y. Liu, and X. Ma, Three-dimensional

flexible electronics using solidified liquid metal with regulated plasticity. *Nat. Electron.* 6, 154 (2023).

17. L. Teng, S.C. Ye, S. Handschuh-Wang, X.H. Zhou, T.S. Gan, and X.C. Zhou, Liquid metal-based transient circuits for flexible and recyclable electronics. *Adv. Funct. Mater.* 29, 1808739 (2019).

18. H.B. An, L.Z. Chen, X.J. Liu, X.Y. Wang, Y.F. Liu, Z.G. Wu, B. Zhao, and H. Zhang, High-sensitivity liquid-metal-based contact lens sensor for continuous intraocular pressure monitoring. *J. Micromech. Microeng.* 31, 035006 (2021).

19. S.H. Jeong, A. Hagman, K. Hjort, M. Jobs, J. Sundqvist, and Z.G. Wu, Liquid alloy printing of microfluidic stretchable electronics. *Lab Chip* 12, 4657 (2012).

20. B.A. Gozen, A. Tabatabai, O.B. Ozdoganlar, and C. Majidi, High-density soft-matter electronics with micron-scale line width. *Adv. Mater.* 26, 5211 (2014).

21. C.F. Pan, E.J. Markvicka, M.H. Malakooti, J.J. Yan, L.M. Hu, K. Matyjaszewski, and C. Majidi, A liquid-metal-elastomer nano-composite for stretchable dielectric materials. *Adv. Mater.* 31, 1900663 (2019).

22. H.W. Bark and P.S. Lee, Surface modification of liquid metal as an effective approach for deformable electronics and energy devices. *Chem. Sci.* 12, 2760 (2021).

23. K.B. Ozutemiz, J. Wissman, O.B. Ozdoganlar, and C. Majidi, EGaIn–metal interfacing for liquid metal circuitry and microelectronics integration. *Adv. Mater. Interfaces* 5, 1701596 (2018).

24. Z.Y. Wang, X.T. Xia, M. Zhu, X.L. Zhang, R. Liu, J. Ren, J.Y. Yang, M. Li, J. Jiang, and Y. Liu, Rational assembly of liquid metal/elastomer lattice conductors for high-performance and strain-invariant stretchable electronics. *Adv. Funct. Mater.* 32, 2108336 (2022).

25. F. Pineda, F. Bottausci, B. Icard, L. Malaquin, and Y. Fouillet, Using electrofluidic devices as hyper-elastic strain sensors: experimental and theoretical analysis. *Microelectron. Eng.* 144, 27 (2015).

26. N. Cohen and K. Bhattacharya, A numerical study of the electromechanical response of liquid metal embedded elastomers. *Int. J. Nonlin. Mech.* 108, 81 (2019).

27. Y.H. Wang and D.L. Henann, Finite-element modeling of soft solids with liquid inclusions. *Extreme Mech. Lett.* 9, 147 (2016).

28. M.D. Dickey, R.C. Chiechi, R.J. Larsen, E.A. Weiss, D.A. Weitz, and G.M. Whitesides, Eutectic gallium-indium (EGaIn): a liquid metal alloy for the formation of stable structures in microchannels at room temperature. *Adv. Funct. Mater.* 18, 1097 (2008).

29. E. Schmid. Yield point of a crystals: critical shear stress law. *Proc. Internat Congr. Appl. Mech.* 342 (1924).

30. Y.P. Jiang and Y. Zhu, Numerical investigation on the piezo-resistive effect of Ga-based liquid metal filled elastomers (LMECs). *J. Electron. Mater.* 53, 499 (2024).

31. Y.P. Jiang, Y. Zhu, and T.Y. Li, Computational micromechanics of the elastic behaviors of liquid metal-elastomer composites. *MRS Commun.* 12, 465 (2022).

32. N.B. Morley, J. Burris, L.C. Cadwallader, and M.D. Nornberg, GaInSn usage in the research laboratory. *Rev. Sci. Instrum.* 79, 056107 (2008).